

Supporting Information

Kagome-Topology 2D Covalent Organic Frameworks Assembled from D_{2h} -Symmetric and Non-Centrosymmetric C_2 -Symmetric Blocks for Photothermal Imaging

Jiahao Li,^{‡a} Guinan Chen,^{‡a} Chunhong Chen,^{‡b} Yuanyuan Lou,^a Zhihao Xing,^a Tao Zhang,^a Chengtao Gong^a, and Yongwu Peng^{*a}

^a College of Materials Science and Engineering, Zhejiang University of Technology, Hangzhou, 310014, China.

^b State Key Laboratory of Organic Electronics and Information Displays & Jiangsu Key Laboratory for Biosensors, Institute of Advanced Materials (IAM), Jiangsu National Synergetic Innovation Center for Advanced Materials (SICAM), Nanjing University of Posts and Telecommunications, Nanjing, China

E-mail: ywpeng@zjut.edu.cn

[‡]J. H. Li, G. N. Chen, and C. H. Chen contributed equally to this work.

Table of Contents

1. Materials and methods.....	S3
2. Synthesis and general procedures.....	S5
2.1. Synthesis and characterization of COFs.....	S5
Figure S1. FT-TR spectra.....	S6
Figure S2. Solid-state ¹³ C CP-MAS NMR spectroscopy.....	S6
Figure S3. TGA curves.....	S7
Figure S4. DSC curves.....	S7
Figure S5. PXRD patterns for different topologies.....	S8
Figure S6. Different stacking models of COF-TA with kgm topology.....	S8
Figure S7. Different stacking models of COF-TA with sql topology.....	S9
Figure S8. Different stacking models of COF-DP with kgm topology.....	S9
Figure S9. Different stacking models of COF-DP with sql topology.....	S10
Figure S10. Energy calculations for COF-TA with different structures.....	S11
Figure S11. Energy calculations for COF-DP with different structures.....	S12
Figure S12. SEM images.....	S13
Figure S13-14. TEM images.....	S14
2.2. Unit cell parameters and fractional atomic coordinates.....	S16
Table S1-2. Unit cell parameters and fractional atomic coordinates.....	S16
2.3. Photothermal conversion capability.....	S20
Figure S15. UV-Vis spectra.....	S20
Figure S16. Mott-Schottky plots.....	S20
Figure S17. Band edge positions.....	S21
Figure S18. Photothermal performance.....	S21
Table S3. Photothermal conversion efficiency.....	S22
3. References.....	S23

1. Materials and methods

All the chemicals are commercially available and used without further purification. All solvents were dried and distilled according to conventional methods. 1,2-dichlorobenzene (*o*-DCB), 1-butanol (n-BuOH), acetone, tetrahydrofuran (THF), and acetic acid (AcOH) were purchased from Sigma-Aldrich. N,N,N',N'-Tetra(*p*-aminophenyl)-*p*-phenylenediamine (TPPDA), 2,3-dimethoxy-1,4-benzenedicarboxaldehyde (TA) and 2,1,3-benzothiadiazole-4,7-dicarboxaldehyde (DP) were purchased from Shanghai Tensus Biotech.

Power X-ray diffraction (PXRD): PXRD patterns were collected on an X-ray diffraction (XRD) system (DX-27mini, China) using Cu K α radiation.

Fourier transform infrared (FT-IR): IR spectrum was measured on an IR spectrometer (Nicolet 6700) between the ranges of 4000 to 400 cm⁻¹.

Solid-state nuclear magnetic resonance (ssNMR): Solid-state nuclear magnetic resonance (NMR) data were performed on a Bruker AVANCE III 600 spectrometer with cross-polarization magic-angle-spinning (CP/MAS) at a resonance frequency of 150.9 MHz. ¹³C CP/MAS NMR spectra were recorded using a 4 mm MAS probe and a spinning rate of 12kHz. A contact time of 4 ms and a recycle delay of 2 s were used for the ¹³C CP/MAS NMR measurement. The chemical shifts of ¹³C were externally referenced to tetramethylsilane (TMS).

Scanning electron microscope (SEM): SEM images were collected using a GeminiSEM 500 system.

Transmission electron microscope (TEM): TEM images were obtained with a Tecnai G2 F30 S-Twin.

Thermogravimetric analysis (TGA): TGA was performed using a TA Q5000 under flowing N₂ with 20 K min⁻¹ ramp rate. Samples were heated in a Platinum pan (700 °C, 20 °C min⁻¹) under a N₂ flux (25 mL min⁻¹).

Differential Scanning Calorimetry (DSC): DSC was performed using a DSC 3500 SIRius under flowing N₂ with 10 K min⁻¹ ramp rate. Samples were heated in a Platinum pan (200 °C, 10 °C min⁻¹) under a N₂ flux (25 mL min⁻¹).

UV-Vis absorption spectra (UV): UV-Vis diffuse reflectance spectra and UV-Vis absorption spectra were performed by using Shimadzu UV-2600i UV VIS-NIR Spectrophotometer.

Crystal structure modeling: Structural modeling of COFs was generated using the Materials Studio^{S1} program employing the *Building (Crystal)* module, the lattice model was geometrically optimized using force-field based method (*Forcite* molecular dynamics module) and SCC-DFTB (*DFTB* + module). The Pawley fitting (*Reflex* module) was performed to optimize the lattice parameters iteratively until the R_{wp} value converges and the overlay of the observed with refined profiles shows good agreement. Powder indexing and Rietveld refinement were performed using EXPO2014^{S2} various topology structures were illustrated by VESTA software^{S3}.

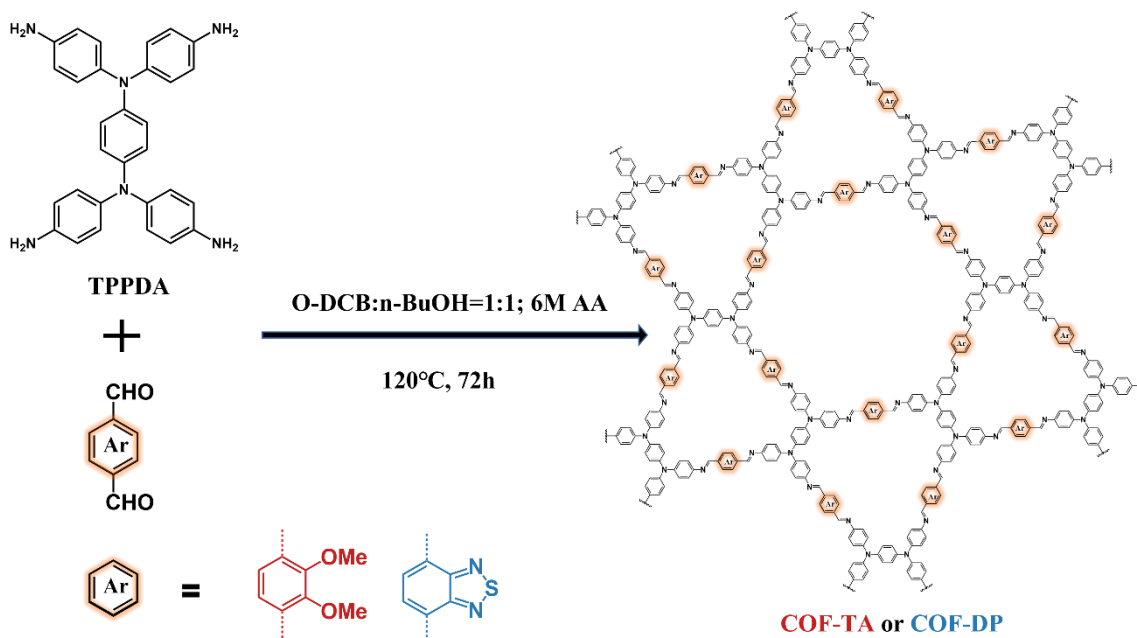
Electrochemical Study: Fluoride-tin oxide (FTO) glasses were firstly cleaned by sonication in ethanol for 30 min and dried under nitrogen flow. 5 mg of COFs powder was mixed with 1 mL ethanol and ultra-sonicated for 2 h to get slurry. 40 μ L of the suspension was drop-casted on the FTO glass and dried in an oven at 60 °C for 30 min. The photocurrent response was measured using a three-electrode setup with a working electrode (COF on FTO glass), counter electrode (Pt wire), and reference electrode (Ag/AgCl). The electrolyte was a 0.5 M Na₂SO₄ aqueous solution and was purged. The photocurrent responses were conducted with an Ivium workstation, with the working electrodes irradiated from the front side and the visible light was generated by LED. Mott-Schottky experiments

were conducted with a perturbation signal of 5 mV at frequencies of 1000, 1500, and 2000 Hz.

Photothermal conversion properties measurement: COF powders were pressed into thin slices with a diameter of 4 mm and then set aside in a quartz petri dish. The corresponding film was spread on a PTFE slide at a distance of 10 cm from the 808 nm laser (Hi-Tech Optoelectronics Co., Ltd, Beijing, China). The power density of the laser was adjusted between 0.1 and 1.0 W cm⁻². Infrared videos of samples were recorded with an IR thermal camera (FLUKE TiS20 Thermal Imaging Camera).

2. Synthesis and general procedures

2.1 Synthesis and characterization of COFs



COF-TA: TPPDA (14.1 mg, 0.03 mmol) and TA (11.6 mg, 0.06 mmol) were added into a glass ampoule with 1,2-dichlorobenzene (0.5 mL) and n-butanol (0.5 mL). The solution was sonicated for 5 minutes to obtain grey turbid solution. 6 M acetic acid (0.1 mL) were added into the glass ampoule as catalyst. The glass ampoule was flash frozen at 77 K using the liquid nitrogen bath and degassed by freeze-pump-thaw three times, and then sealed. The glass ampoule was placed in an oven at 120 °C for 3 days. The yellow solid was isolated by centrifugation and washed with N, N-dimethylacetamide (3×10 mL) and acetone (3×10 mL). The resulting precipitate was filtered then exhaustively washed with tetrahydrofuran and acetone by Soxhlet extraction for 48 hours. The sample was then transferred to vacuum chamber and evacuated to 20 mTorr at 80 °C for 24 h, yielding yellow powder COF-TA (Yield: 23.0 mg, 85.5%).

COF-DP: TPPDA (14.1 mg, 0.03 mmol) and DP (11.6 mg, 0.06 mmol) were added into a glass ampoule with 1,2-dichlorobenzene (0.25 mL) and Benzyl alcohol (0.75 mL). The solution was sonicated for 5 minutes to obtain grey turbid solution. 6 M acetic acid (0.1 mL) were added into the glass ampoule as catalyst. The glass ampoule was flash frozen at 77 K using the liquid nitrogen bath and degassed by freeze-pump-thaw three times, and then sealed. The glass ampoule was placed in an oven at 120 °C for 3 days. The yellow solid was isolated by centrifugation and washed with N, N-dimethylacetamide (3×10 mL) and acetone (3×10 mL). The resulting precipitate was filtered then exhaustively washed with tetrahydrofuran and acetone by Soxhlet extraction for 48 hours. The sample was then transferred to vacuum chamber and evacuated to 20 mTorr at 80 °C for 24 h, yielding black powder COF-DP (Yield: 22.4 mg, 87.1%).

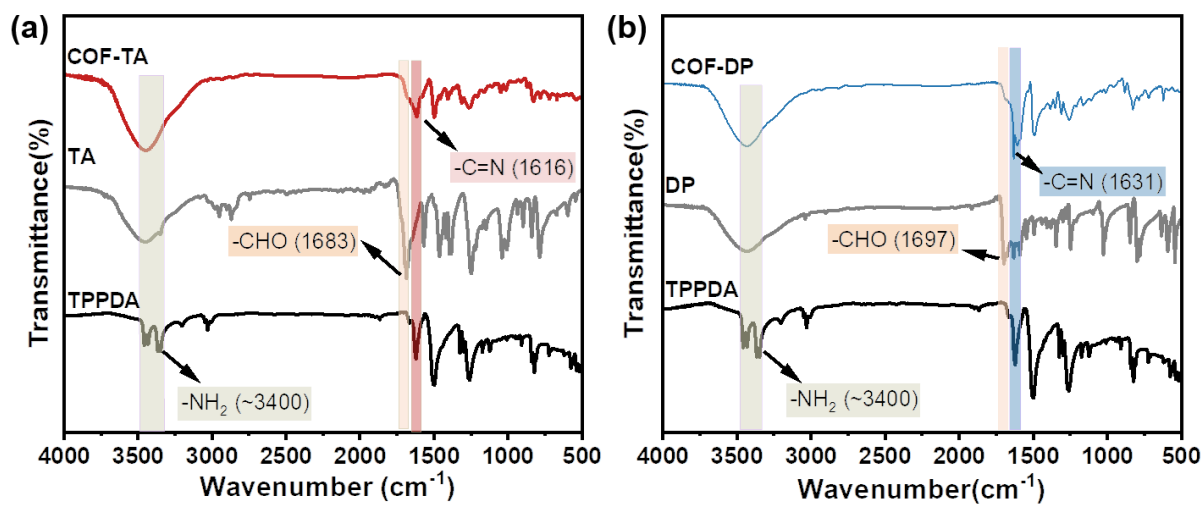


Figure S1. FT-IR spectra of (a) COF-TA and (b) COF-DP.

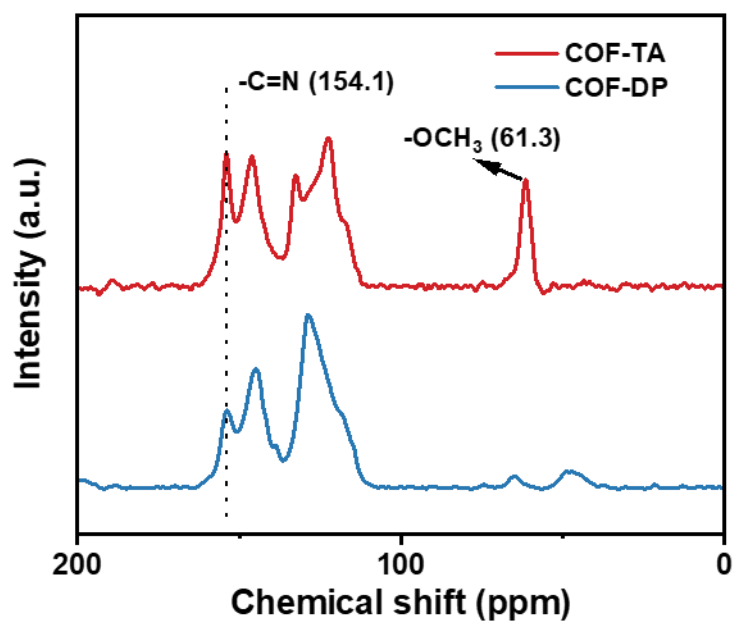


Figure S2. ^{13}C CP/MAS NMR spectra of COF-TA and COF-DP.

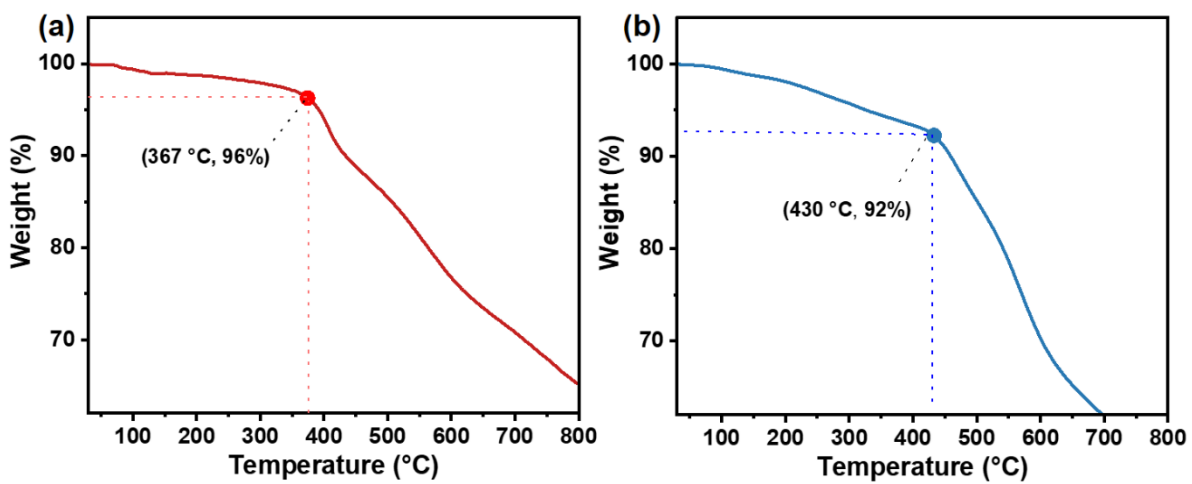


Figure S3. TGA curves of (a) COF-TA and (b) COF-DP.

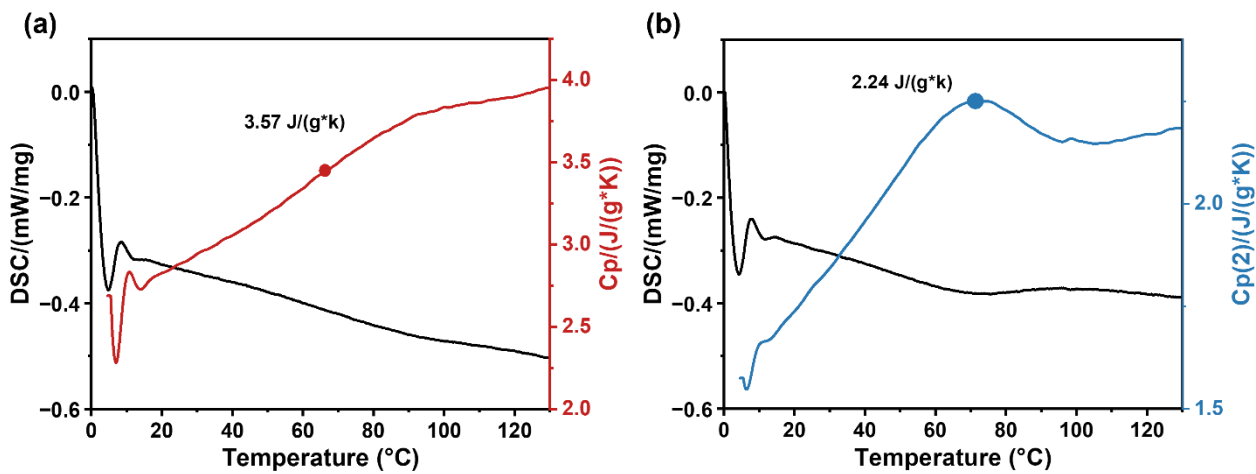


Figure S4. DSC curves of (a) COF-TA and (b) COF-DP.

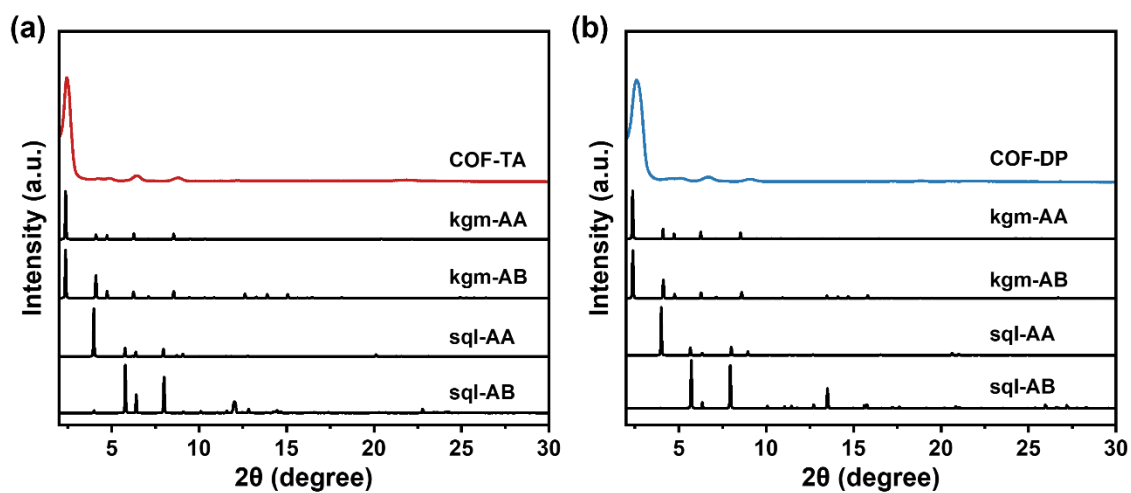


Figure S5. Experimental and Simulated PXRD patterns of (a) COF-TA and (b) COF-DP with different topologies and stacking models.

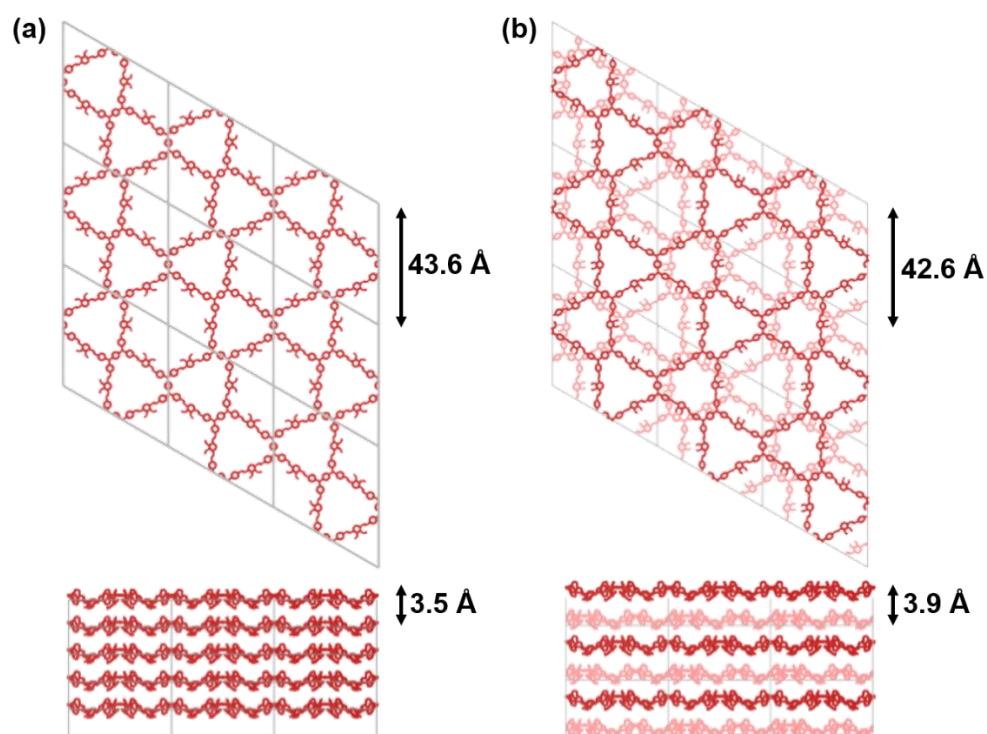


Figure S6. Different stacking models for COF-TA with kgm topology, showcasing (a) AA stacking (denoted as kgm-AA) and (b) AB stacking (denoted as kgm-AB).

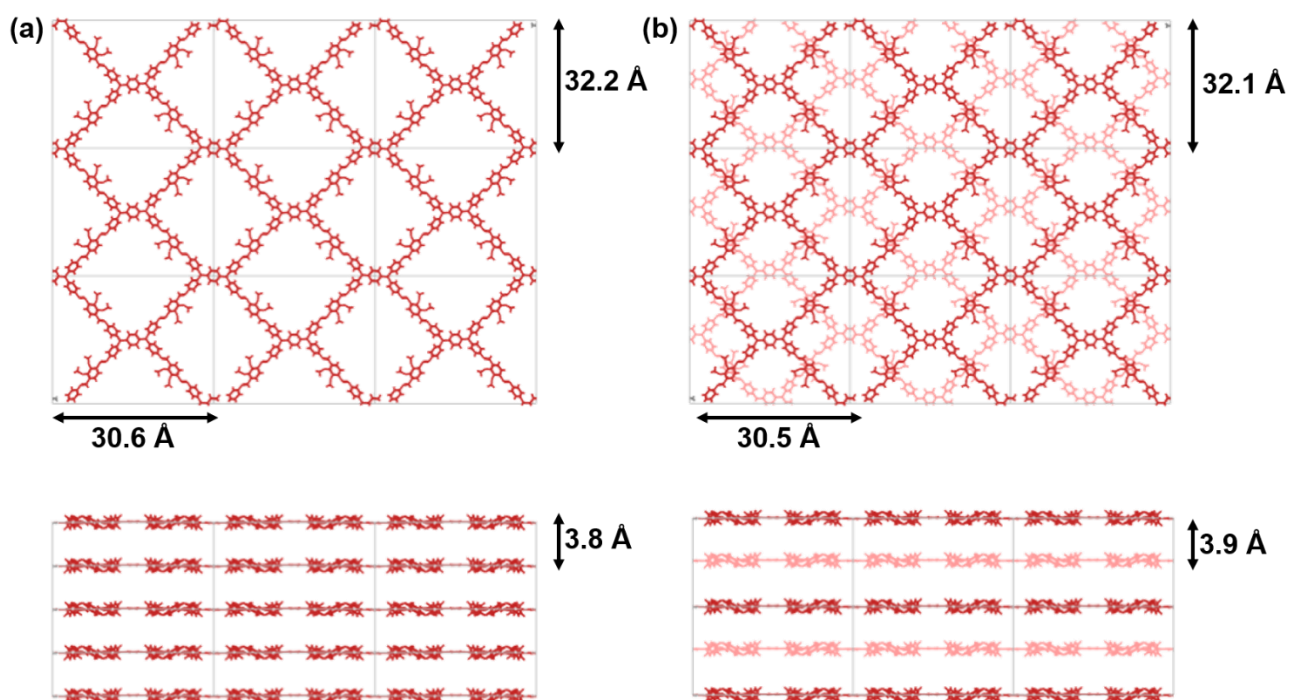


Figure S7. Different stacking models for COF-TA with sql topology, showcasing (a) AA stacking (denoted as sql-AA) and (b) AB stacking (denoted as sql-AB).

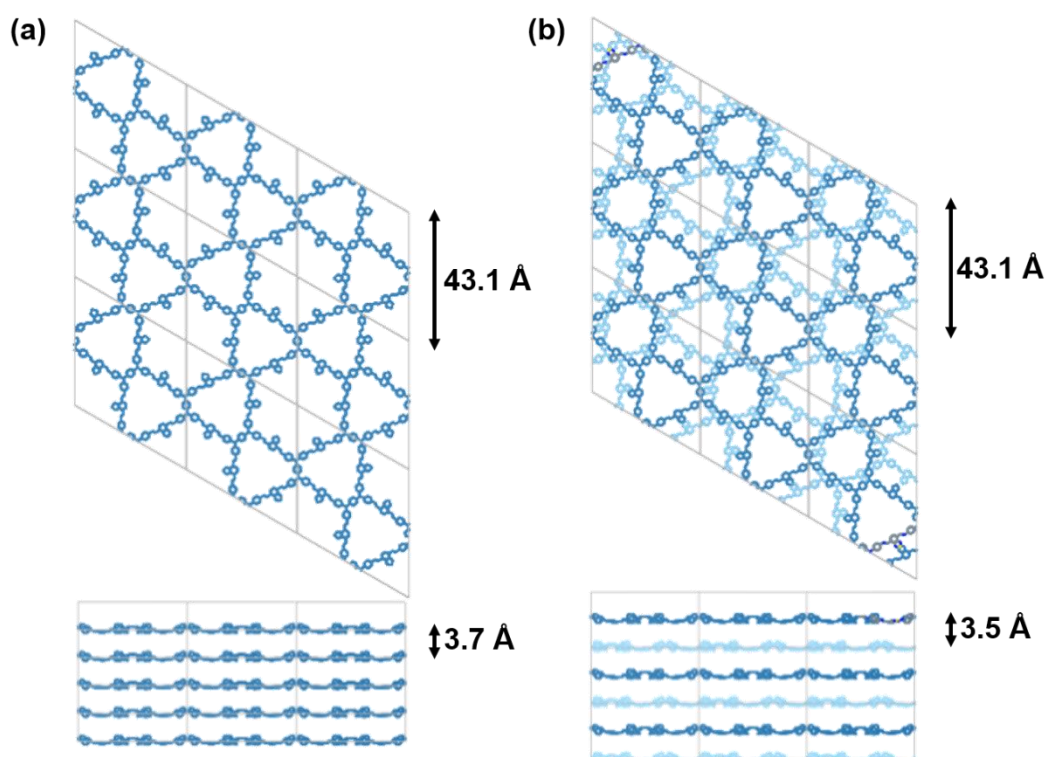


Figure S8. Different stacking models for COF-DP with kgm topology, showcasing (a) AA stacking (kgm-AA) and (b) AB stacking (kgm-AB).

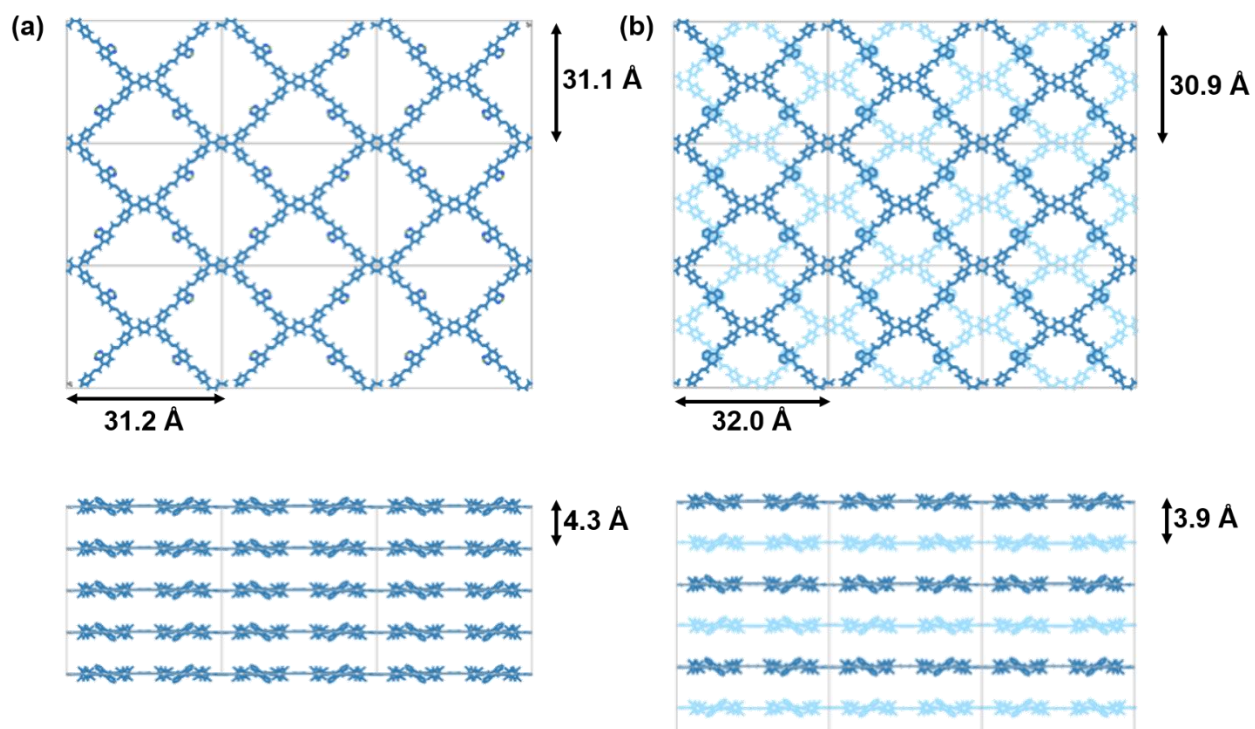


Figure S9. Different stacking models for COF-DP with sql topology, showcasing (a) AA stacking (sql-AA) and (b) AB stacking (sql-AB).

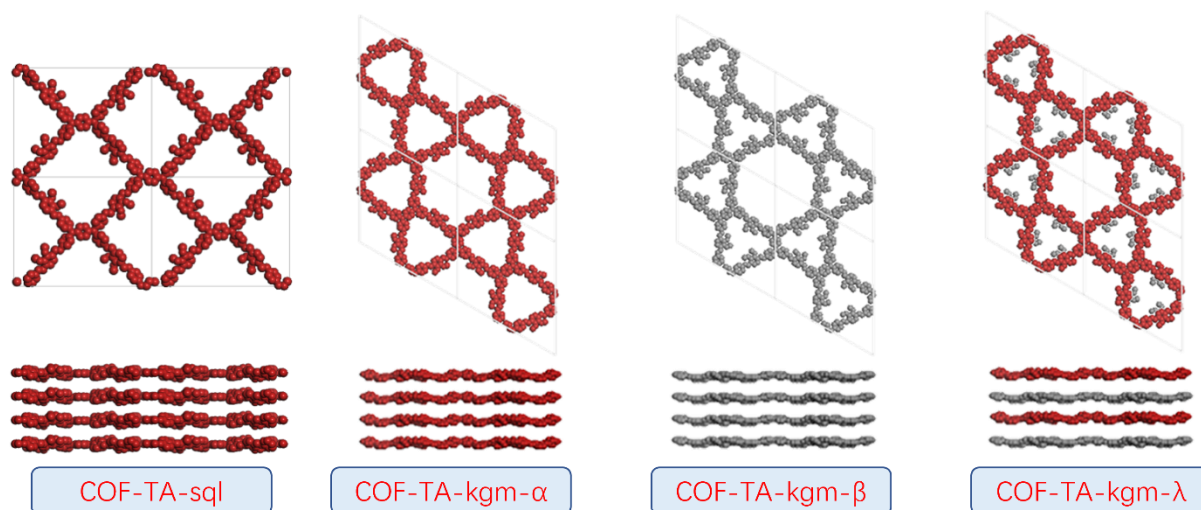


Figure S10. COF-TA with different stacking models for energy calculation.

We investigated the interlayer stacking energy of possible structures for **COF-TA** based on sql and kgm topologies. Four distinct structures were considered: **COF-TA-sql**, featuring AA-stacked sql topology, and three kgm-based structures: **COF-TA-kgm- α** , where all methoxy groups point towards the small holes; **COF-TA-kgm- β** , with all methoxy groups directed towards the macropores; and **COF-TA-kgm- λ** , exhibiting even distribution of methoxy groups in both pores (anti-parallel stacking). The total energy relative values for these structures were calculated using the COMPASS II force field in Forcite of Material Studio 7.0, yielding values of 51.0, 34.0, 115.0, and 0 kJ/mol, respectively. These results indicate that the COF-TA-kgm- λ structure, characterized by anti-parallel stacking in the kgm topology, is the most thermodynamically stable product.

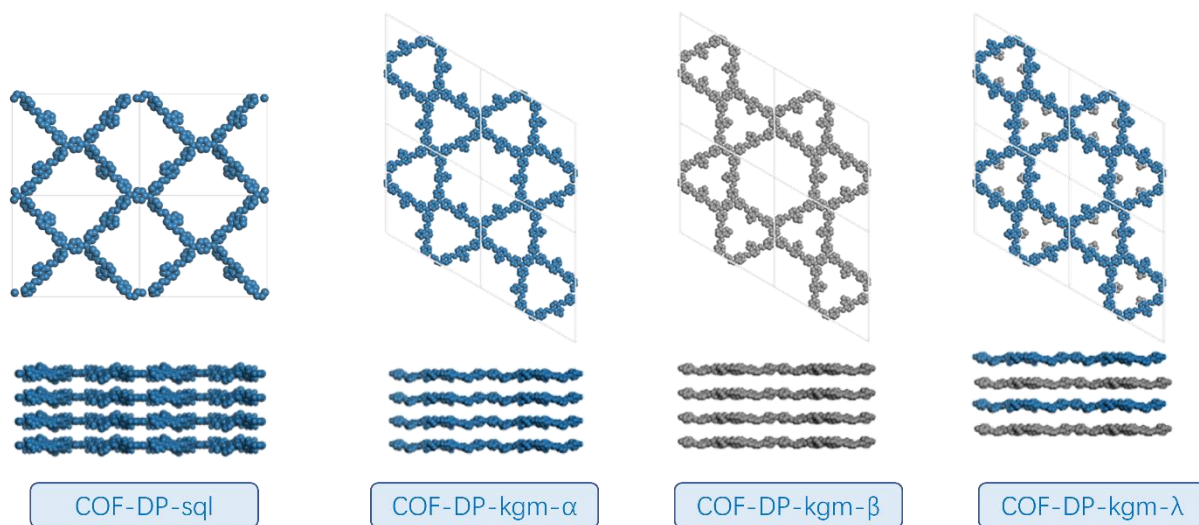


Figure S11. COF-DP with different stacking models for energy calculation.

Similarly, we investigated the interlayer stacking energy of possible structures for **COF-DP** based on sql and kgm topologies. Four distinct structures were considered: **COF-DP-sql**, featuring AA-stacked sql topology, and three kgm-based structures: **COF-DP-kgm- α** , where all thiadiazole groups point towards the small holes; **COF-DP-kgm- β** , with all thiadiazole groups directed towards the macropores; and **COF-DP-kgm- λ** , exhibiting even distribution of thiadiazole groups in both pores (anti-parallel stacking). The total energy relative values for these structures were calculated using the COMPASS II force field in Forcite of Material Studio 7.0, yielding values of 36.0, 129.0, 127.0 and 0 kJ/mol, respectively. These results indicate that the COF-DP-kgm- λ structure, characterized by anti-parallel stacking in the kgm topology, is the most thermodynamically stable product.

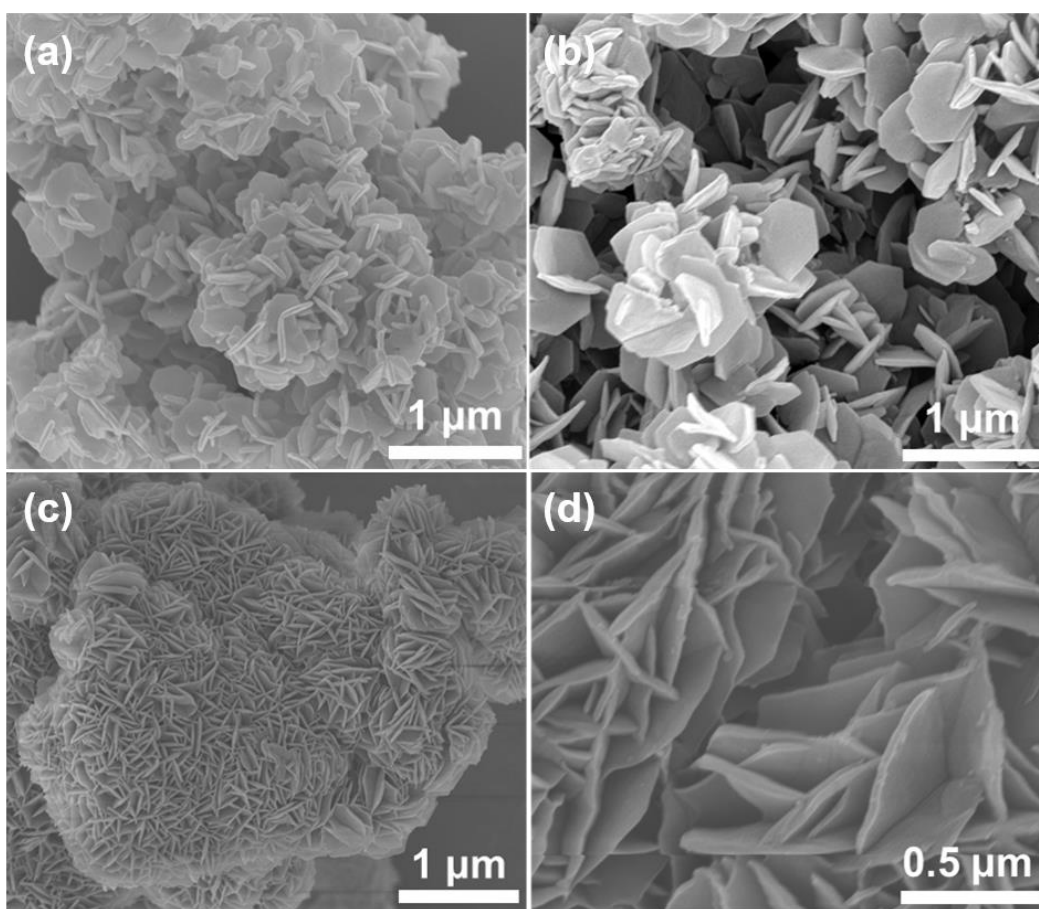


Figure S12. SEM images of (a, b) COF-TA and (c, d) COF-DP.

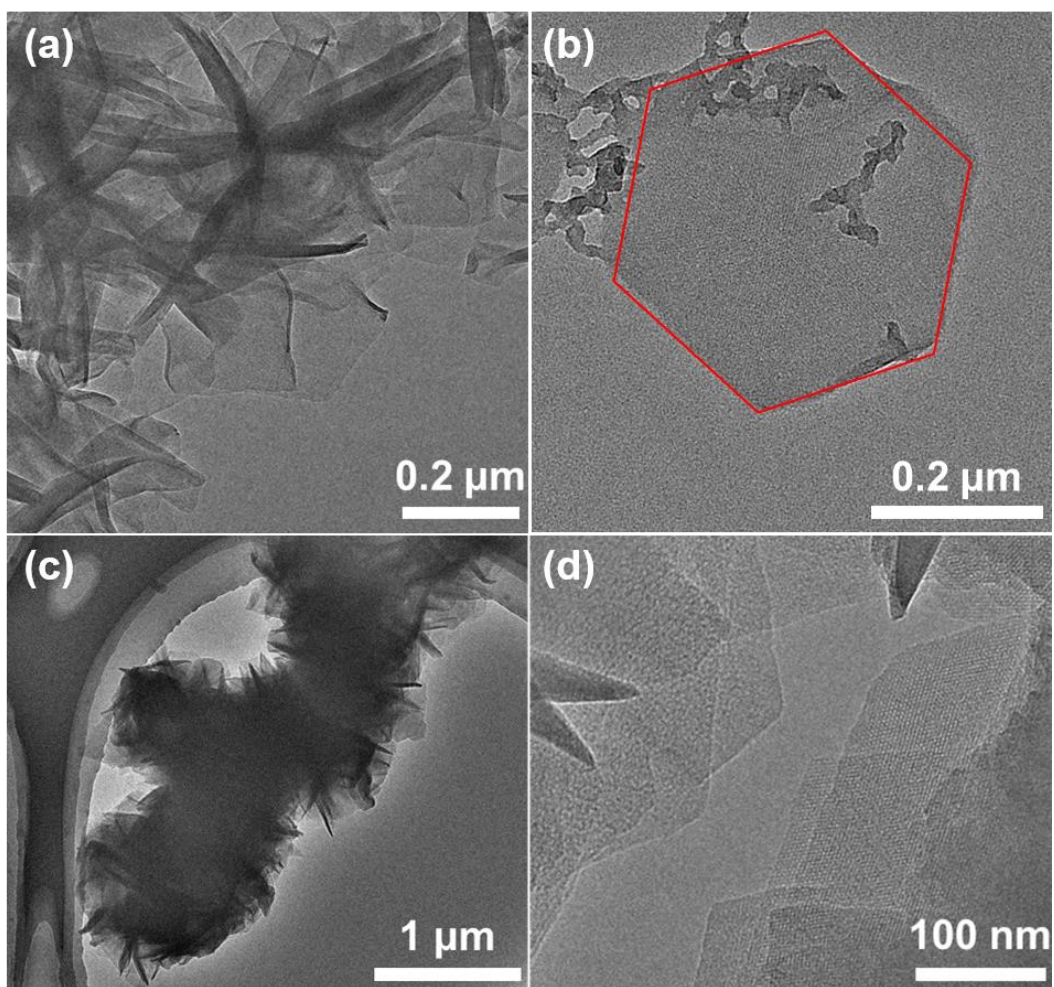


Figure S13. TEM images of (a, b) COF-TA and (c, d) COF-DP.

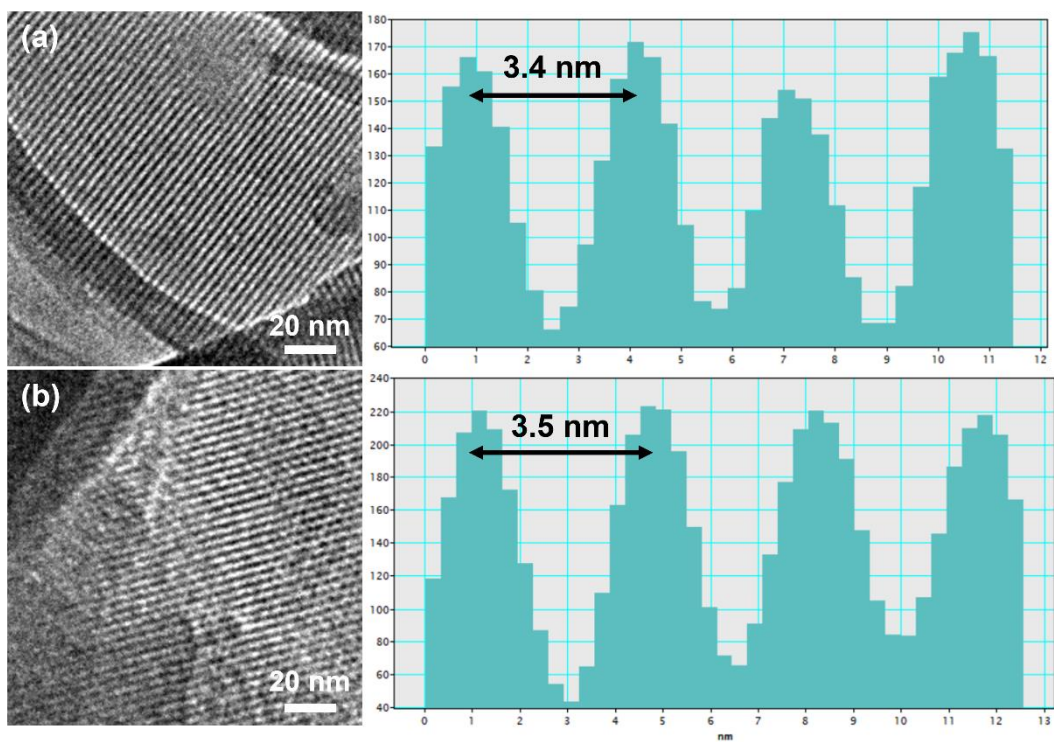


Figure S14. TEM images and corresponding intensity profiles of (a) **COF-TA** and (b) **COF-DP**, highlighting distinct lattice fringes aligned with the [100] crystallographic plane in both COFs.

2.2 Unit cell parameters and fractional atomic coordinates

Table S1. Unit cell parameters and fractional atomic coordinates for COF-TA calculated based on kgm topology with antiparallel stacking.

Space group		<i>P6/M</i>	
Calculated unit cell		$a = 43.6 \text{ \AA}; b = 43.6 \text{ \AA}; c = 3.5 \text{ \AA}$ $\alpha = \beta = 90^\circ; \gamma = 120^\circ$	
Atoms	X	Y	Z
N	0.56	0.57	0
C	0.6	0.58	0
C	0.63	0.61	0
C	0.66	0.61	0
C	0.67	0.58	0
C	0.64	0.55	0
C	0.6	0.55	0
N	0.7	0.59	0
C	0.7	0.56	0
C	0.74	0.56	0
C	0.77	0.59	0
C	0.8	0.59	0
C	0.8	0.56	0
C	0.77	0.53	0
C	0.74	0.52	0
C	0.84	0.57	0
N	0.85	0.54	0
C	0.89	0.55	0
C	0.92	0.58	0
C	0.95	0.59	0
C	0.96	0.56	0
C	0.93	0.53	0
C	0.89	0.52	0
C	0.53	0.54	0
C	0.53	0.5	0
C	0.5	0.47	0

N	0.56	0.57	0.5
C	0.6	0.57	0.5
C	0.63	0.61	0.5
C	0.66	0.61	0.5
C	0.67	0.58	0.5
C	0.64	0.55	0.5
C	0.6	0.55	0.5
N	0.7	0.59	0.5
C	0.71	0.57	0.5
C	0.75	0.57	0.5
C	0.78	0.61	0.5
C	0.82	0.61	0.5
C	0.82	0.58	0.5
C	0.78	0.54	0.5
C	0.75	0.54	0.5
C	0.85	0.58	0.5
N	0.85	0.55	0.5
C	0.89	0.55	0.5
C	0.92	0.58	0.5
C	0.95	0.59	0.5
C	0.96	0.56	0.5
C	0.92	0.53	0.5
C	0.89	0.52	0.5
C	0.53	0.53	0.5
C	0.53	0.5	0.5
C	0.5	0.47	0.5
O	0.15	0.36	0.5
O	0.21	0.36	0.5
C	0.12	0.35	0.5
C	0.24	0.35	0.5
O	0.23	0.51	1
O	0.29	0.51	1
C	0.21	0.52	1
C	0.33	0.51	1

Table S2. Unit cell parameters and fractional atomic coordinates for **COF-DP** calculated based on kgm topology with antiparallel stacking.

Space group		<i>P6/M</i>	
Calculated unit cell		$a = b = 43.1 \text{ \AA}; c = 3.7 \text{ \AA}$ $\alpha = \beta = 90^\circ; \gamma = 120^\circ$	
Atoms	X	Y	Z
N	0.23	0.5	1
S	0.28	0.54	1
N	0.56	0.57	0
C	0.6	0.58	0
C	0.63	0.61	0
C	0.66	0.61	0
C	0.67	0.58	0
C	0.64	0.55	0
C	0.6	0.55	0
N	0.7	0.59	0
C	0.7	0.56	0
C	0.74	0.56	0
C	0.77	0.59	0
C	0.8	0.59	0
C	0.81	0.56	0
C	0.77	0.53	0
C	0.74	0.52	0
C	0.84	0.57	0
N	0.85	0.54	0
C	0.89	0.55	0
C	0.92	0.58	0
C	0.95	0.59	0
C	0.96	0.56	0
C	0.93	0.53	0
C	0.89	0.52	0
C	0.53	0.54	0
C	0.53	0.5	0

C	0.5	0.47	0
N	0.56	0.57	0.5
C	0.6	0.58	0.5
C	0.63	0.61	0.5
C	0.66	0.61	0.5
C	0.67	0.58	0.5
C	0.64	0.55	0.5
C	0.61	0.55	0.5
N	0.7	0.59	0.5
C	0.71	0.57	0.5
C	0.75	0.57	0.5
C	0.78	0.61	0.5
C	0.82	0.61	0.5
C	0.82	0.58	0.5
C	0.79	0.54	0.5
C	0.75	0.54	0.5
C	0.85	0.58	0.5
N	0.85	0.55	0.5
C	0.89	0.55	0.5
C	0.92	0.59	0.5
C	0.95	0.59	0.5
C	0.96	0.56	0.5
C	0.93	0.53	0.5
C	0.89	0.52	0.5
C	0.53	0.54	0.5
C	0.53	0.5	0.5
C	0.51	0.47	0.5
N	0.16	0.36	0.5
N	0.21	0.36	0.5
S	0.17	0.33	0.5
N	0.29	0.51	1

2.3 Photothermal conversion capability

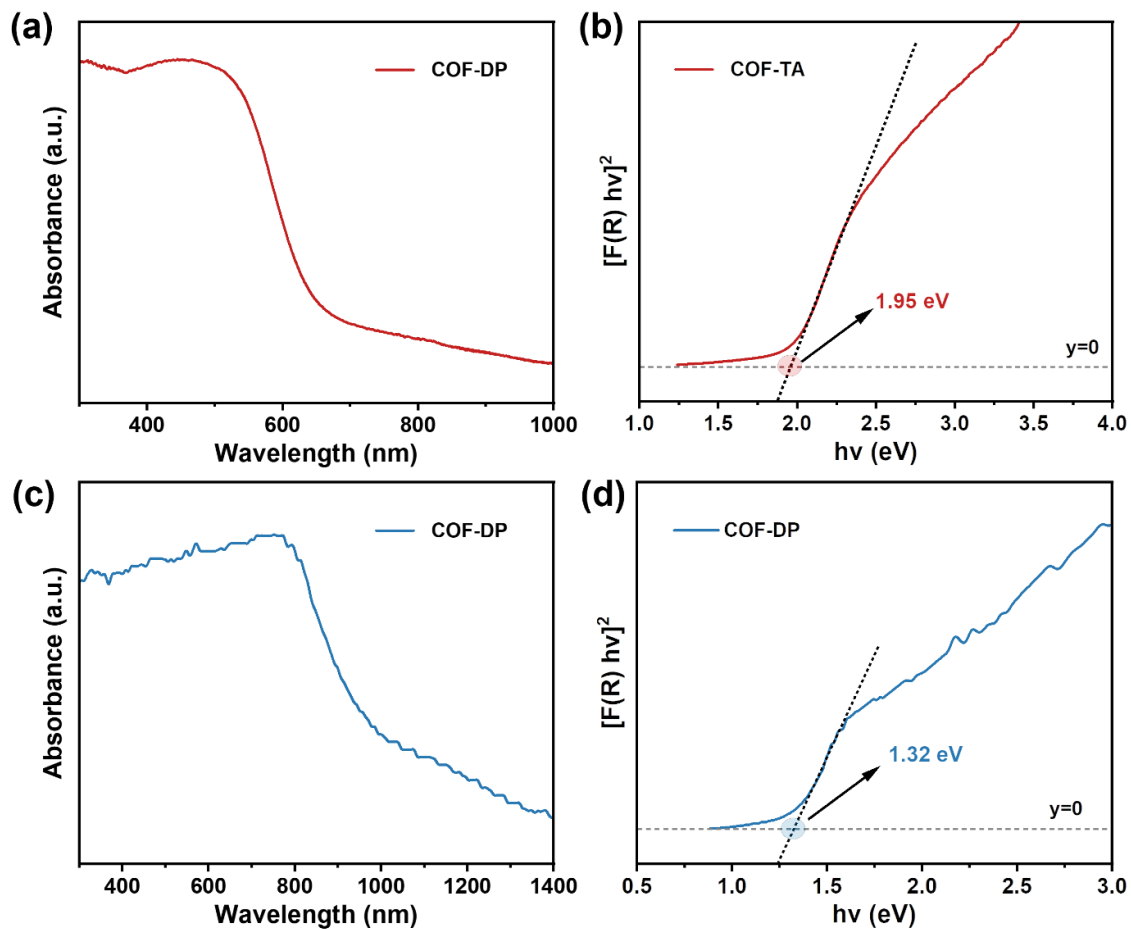


Figure S15. UV-Vis absorption spectra and plots of the Kubelka-Munk function of (a, b) COF-TA and (c, d) COF-DP.

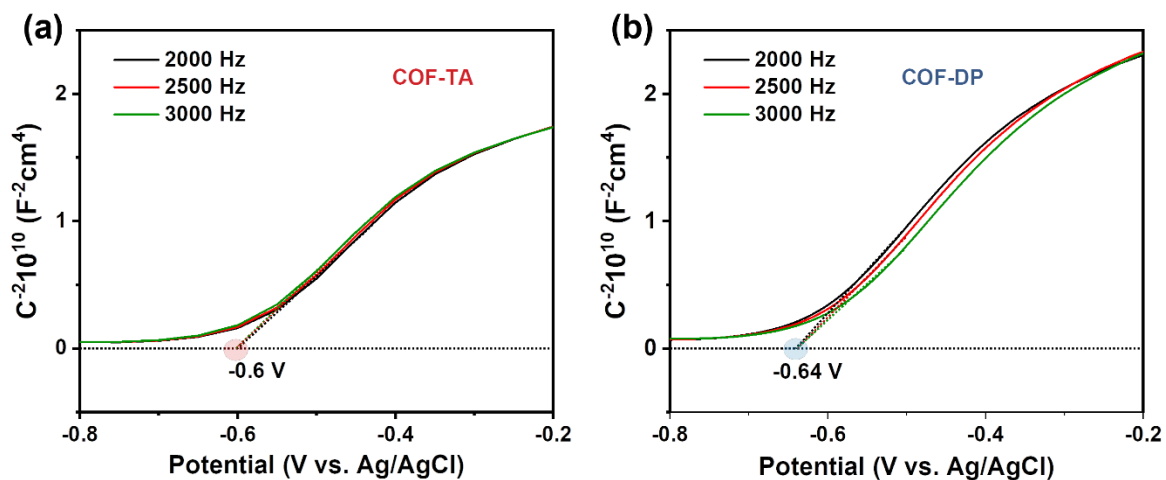


Figure S16. Mott-Schottky plots of (a) COF-TA and (b) COF-DP.

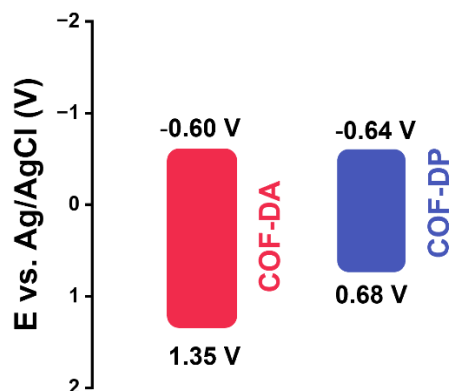


Figure S17. Band edge positions of COF-TA and COF-DP.

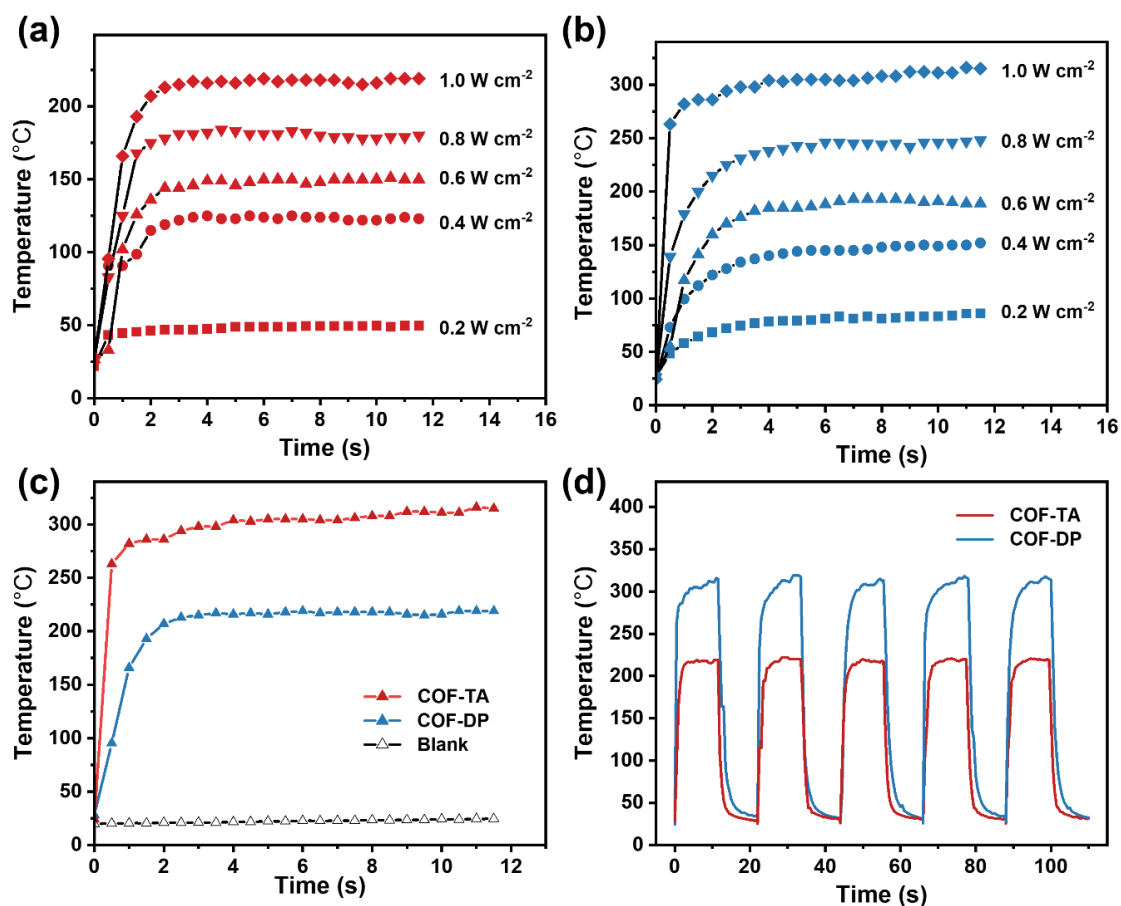


Figure S18. Time-dependent temperature profiles of (a) COF-TA and (b) COF-DP upon illumination with varying power densities (0.2, 0.4, 0.6, 0.8 and 1.0 W/cm²). (c) Comparative analysis of temperature changes between COF-TA, COF-DP, and a blank control when exposed to 880 nm laser at 1.0 W/cm². (d) Thermal cycling behavior of COFs during repeated NIR illumination at 1.0 W/cm².

Calculation of the photothermal conversion efficiency^{S4}

The efficiency of photothermal conversion of COF samples (COF-TA and COF-DP) is determined by calculating the total thermal energy generated by the samples and dividing it by the input light energy. The thermal energy (Q) can be calculated using the equation:

$$Q=cm\Delta T$$

Where ΔT represents the temperature increase, m is the mass, and c is the specific heat capacity of the COF samples (shown in Fig. S3).

The total input energy density applied to the COF samples can be expressed as:

$$E=pst$$

where p is the input power density of light, s is the irradiation area, and t is the irradiation time.

The energy efficiency (η) of the COF samples is estimated as:

$$\eta=\frac{Q}{E}=\frac{cm\Delta T}{PSt}$$

Therefore, the efficiency of the photothermal conversion under NIR light could be estimated to be:

$$\eta_{\text{COF-TA}}=\frac{Q}{E}=\frac{3.57\times 0.016\times 216}{1\times 1\times 2}=6.17\% \text{ and } \eta_{\text{COF-DP}}=\frac{Q}{E}=\frac{2.24\times 0.016\times 311}{1\times 1\times 1}=11.15\%.$$

Table S3. Photothermal conversion efficiencies of COF-TA and COF-DP.

COFs sample	c (J g ⁻¹ ·K ⁻¹)	m (g)	ΔT (°C)	p (W cm ⁻²)	s (cm ²)	t (s)	η (%)
COF-TA	3.57	0.016	216	1.0	1.0	2	6.17
COF-DP	2.24	0.016	311	1.0	1.0	1	11.15

3. References

(S1) Materials Studio; Accelrys: San Diego.

(S2) <http://www.ba.ic.cnr.it/softwareic/expo/>

(S3) <http://www.jp-minerals.org/vesta/en/>

(S4) H. Li, H. Wen, Z. Zhang, N. Song, R. Kwok, J. Lam, L. Wang, D. Wang, B. Tang, *Angew. Chem. Int. Ed.*, 2020, **59**, 20371.